X-ray-diffraction studies of the three-dimensional structure within iodine-intercalated poly(3-octylthiophene)

T.J. Prosa and M.J. Winokur
Department of Physics, University of Wisconsin, Madison, Wisconsin 53706

Jeff Moulton and Paul Smith
Department of Materials Science, University of California, Santa Barbara, California 93105

A.J. Heeger
Department of Physics, University of California, Santa Barbara, California 93105
(Received 7 March 1994; revised manuscript received 26 July 1994)

Comprehensive x-ray-diffraction data and structure factor calculations are presented for oriented poly(3-octylthiophene) films intercalated by iodine vapor to I_3^- concentrations of 0, 4, 14, 26, and 45 mol wt. % per octylthiophene monomer. These data reconfirm previous reports that this polymer-iodine complex exhibits a continuous and reversible structural evolution [M.J. Winokur, P. Wamsley, J. Moulton, P. Smith, and A. J. Heeger, Macromolecules **24**, 3812 (1991); T. J. Prosa, M. J. Winokur, J. Moulton, P. Smith, and A. J. Heeger, Synth. Met. **55**, 370 (1993); J. Moulton and P. Smith, *ibid.* **40**, 13 (1991)]. Structure factor modeling calculations are used to fully specify the overall changes in the three-dimensional host polymer structure. This molecular restructuring involves both translational and rotational rearrangements of the host polymer. The fundamental lamellar base structure of the pristine host polymer is found to remain fully intact throughout the entire structural transformation. The large-scale changes in the observed interlayer repeat distances result from continuous variations in the angular orientation of the polymer backbone and in the average position of the alkyl side chains. Translational displacements of the polymer chains parallel to the main chain axes are found to occur within individual lamellae and this motion creates essentially one-dimensional intercalant channels perpendicular to the main chain axis. This latter process facilitates iodine intercalation and is, in part, responsible for the ability to achieve the very high iodine concentrations which have been measured experimentally. Scattering features are seen at the highest iodine concentrations which are indicative of additional structural ordering by the intercalant within the newly formed one-dimensional columns.

I. INTRODUCTION

Poly(3-alkylthiophene)s (P3AT's), and conducting polymers in general, continue to receive considerable attention for their novel electrical and physical properties.[1–5] Despite the many extensive investigations, a comprehensive framework for fully understanding the origin of these properties remains incomplete. One important obstacle to formulating this overall picture, especially in the case of P3AT's, is simply the absence of a detailed understanding of the basic molecular microstructure.

P3AT's are simple linear π-conjugated polymers that have had flexible alkyl side chains chemically anchored at either the 3 or 3′ carbon position [see Fig. 1(a)]. This substitution enables conventional polymer processing methodologies to be utilized while allowing for retention or, in some cases, enhancement of the electronic properties. Many groups have proposed structural models for P3AT's based on observed x-ray-diffraction data.[6–20] All of these studies support a lamellar base structure in which parallel stacks of the polymer main chains are separated by regions filled by the alkyl side chains [see Fig. 1(b)]. Of these studies, only a few attempts have been made to obtain more quantitative results.[6,7,15,19,20] Diffraction studies of these polymers do not lend themselves easily to straightforward structure determinations. The inherent nature of typical host materials (i.e., small crystalline fractions, short coherence lengths, multiple phases, and paracrystallinity) produce diffraction profiles that characteristically consist of a few broad Bragg diffraction peaks superimposed upon a significant noncrystalline scattering background. Continuing improvements in design, synthesis, and processing[21–24] will undoubtedly improve the quality of diffraction data available. However, there still remains a pressing need to unambiguously identify key structural elements in existing host materials both in their original state and after intercalation by a guest specie.

This ability to alter poly(3-octylthiophene) (P3OT), by means of intercalation, is in essence a rigorous test for specifying the polymer microstructure. Addition of an intercalant, by chemical or electrochemical methods, further modifies the host polymer structure so that new scattering information from closely related structures may be obtained. Continuous structural evolution of P3OT, by iodine vapor, has been demonstrated,[1,6,7] and these composite structures exhibit strongly varying x-ray-scattering profiles even at minimal iodine concen-

0163-1829/95/51(1)/159(10)/$06.00 ©1995 The American Physical Society

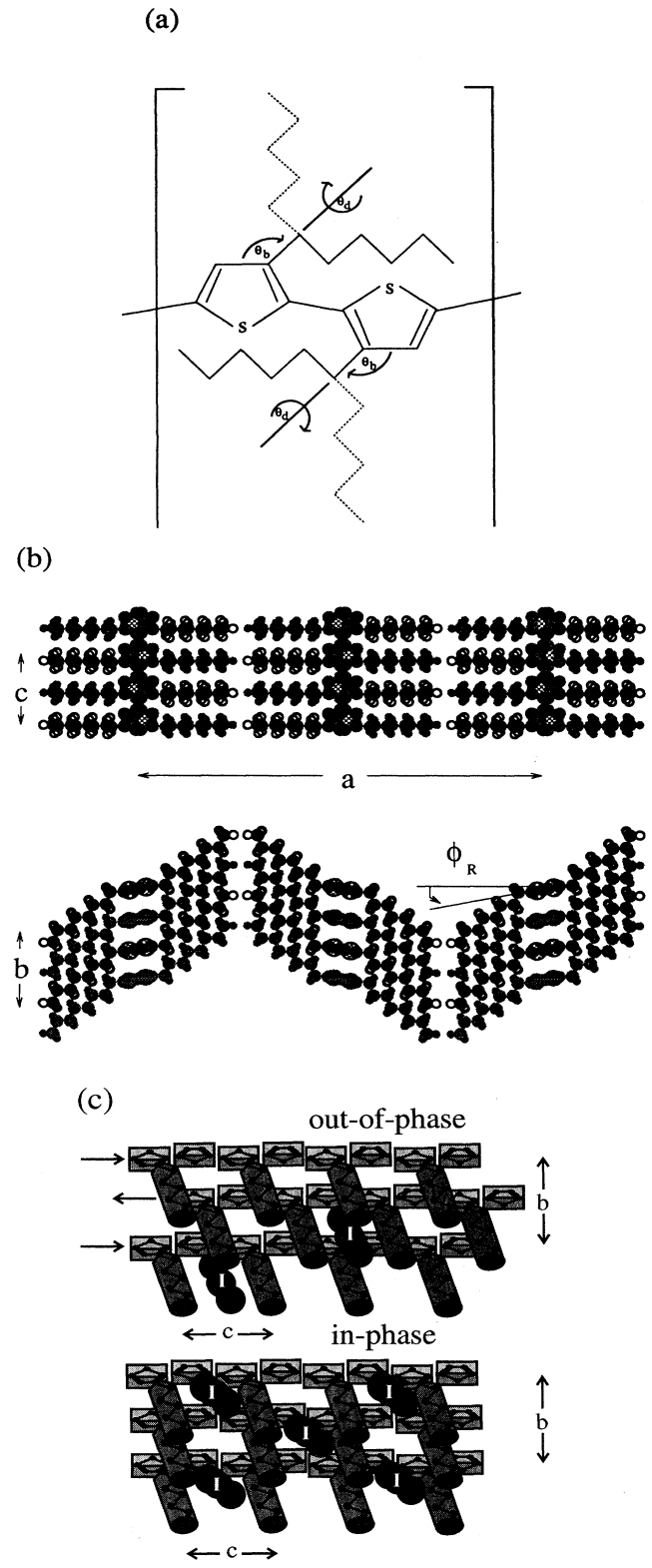

FIG. 1. Various views of P3OT structure and the modeling degrees of freedom: (a) The chemical structure of P3OT; (b) two different projections of the P3OT lamellar packing; (c) packing of side chains for undoped lightly doped (top) and heavily doped P3OT (bottom).

trations. This additional structural information dramatically reduces the number of possible structural models by requiring that any proposed structure must accurately reproduce all scattering features in both intercalated and pristine samples.

In this paper we present experimental data and a refined model for P3OT that fully describes the dominant structural evolution of this polymer during iodine intercalation (or doping) within the crystalline components. The current data reaffirm the continuous doping transformation reported previously,[6,7] but our much improved equatorial scattering data in combination with detailed, nonequatorial data and enhanced modeling techniques requires a fundamental change in the proposed structural evolution of the iodine/P3OT composite. The lamellar polymer stacks are still found to undergo dramatic changes in the average orientation of both the polymer backbone and alkyl side chains, but there is never any indication of a significant alkyl side chain interdigitation between adjacent stacks. Changes in the main chain tilt, ϕ_R, the side chain orientation, θ_d and θ_b, and the ability for the iodine to successfully intercalate into the polymer matrix account for the observed lattice parameter variations, while reorganization of the chain-to-chain packing within individual stacks (parallel to the polymer chain axis) to form essentially one-dimensional columns and the reorganization of the polyiodide ions within these columns adequately accounts for all newly observed features in the scattering profiles.

II. EXPERIMENTAL TECHNIQUES

The P3OT samples utilized in this study were obtained by a direct oxidative coupling of 3-octylthiophene with $FeCl_3$.[4] After synthesis, the $FeCl_3$ was extracted and the films dissolved in chloroform. These solutions were then filtered and immediately poured directly onto glass slides. After solvent evaporation, the films were lifted by methanol and clamped into a simple stretching device. Uniaxial stretching ratios of ~4:1 were typically achieved at drawing temperatures ~ 100 °C, producing film thicknesses of approximately 40 μm.[1]

These films were then mounted into a stainless steel and glass *in situ* vapor doping cell which contained separate sample and iodine source chambers. Both chambers were equipped with independent temperature controllers and could be fully isolated at any time by closing an intervening valve. Evacuation of the entire cell, prior to experimentation, was made possible by a pair of x-ray compatible composite mica/epoxy/beryllium windows. The ability to control the temperature of the polymer and the dopant separately provided for ample control of the doping kinetics. The temperature of the polymer was maintained at 50 °C for all presented data. The temperature of the polymer was increased to as high as 85 °C prior to these scans. A single 5-μm-diam nickel wire was also simultaneously mounted at the polymer surface. This enabled a straightforward determination of iodine concentration by periodically monitoring the intensity of the Ni(111) Bragg reflection. I_3^- is assumed

to be the most prevalent iodine anion because of prior Mössbauer[25–27] and x-ray[28] studies of a related conducting polymer, polyacetylene, and because of simple free volume considerations with the intercalant channels, although a recent study of aqueous iodine-doped P3OT has found that I_5^- is the major constituent in "fully" doped samples.[8] For simplicity, the iodine concentrations have been referenced throughout this paper to a presupposed, all I_3^- composition, but the presence of other polyiodide anion species cannot be ruled out.

The x-ray-diffraction facility consisted of a rotating anode x-ray generator fitted with a Cu target ($\lambda_{K\alpha}$=1.542 Å), a vertically bent HOPG graphite monochrometer, a four-circle diffractometer, and a linear diode array detector. The cross-sectional area of the x-ray beam incident at the sample was adjusted to approximately 2.0×2.0 mm^2. The detector's spatial resolution was set by forming 240 groups of 4 pixels each from the detector's 960 accessible 25 μm × 2 mm pixels. This diode array was located ~30 cm from the scattering center and subtended a 2θ arc of ~4.5°. Typical counting rates for a single group at the most intense reflection were in excess of 200 counts per second per 4 pixel group. In order to minimize nonlinearities across the detector, a correction factor for each group was included and the 2θ step size for each individual data collection point was limited to less than 0.5° (typically 0.3°).

In all cases, radial θ-2θ scans were performed with the sample mounted within the Eulerian cradle. By repositioning the sample both equatorial and nonequatorial scattering could be acquired. For nonequatorial scattering, the sample was maintained in a symmetrical transmission geometry and the **c**-axis angle, with respect to the scattering plane of the detector, set at 5° increments from parallel to perpendicular. The resulting data were then mapped into a single image by drawing constant x-ray intensity contours. These data approximate one quadrant of a conventional flat-film photograph but without the geometrical distortions intrinsic to the film technique. Collection times varied for different data sets, but the complete data collection time at each iodine concentration generally averaged about 2 days. Reproducibility of the individual scans over this time span was excellent.

The structural modeling and calculation of the associated structure factors (SF's) closely follow the procedures outlined in Ref. 19. The local P3OT degrees of freedom employed by this study are a superset of those used previously and include changes in lattice parameters, rotation about the polymer chain axis (a setting angle ϕ_R), rotation of the alkyl side chain about the C-C bond which connects the alkyl chain to the backbone (a dihedral angle θ_d), and changes in the C-C bond angle (a bond angle θ_b). The basic orthorhombic (or monoclinic) unit cells referenced herein invoke an arbitrary doubling of the interlayer spacing in order to esthetically include the two rotationally equivalent layer structures. At intermediate iodine doping levels a mixed phase model was employed where different amounts of "in-phase" (IP) and "out-of-phase" (OP) stacking were utilized [see Fig. 1(c)]. This additional feature provides only slight improvements in the modeling results over a simple all IP then all OP doping sequence. Additional parameters were necessary to account for iodine contributions to the scattering profiles. These factors included positional and orientational degrees of freedom in combination with a fractional site occupancy. Various species of molecular iodine were also tested. These included I_3^- and I_5^-, but the best fits, at low iodine concentrations, were realized using an I_3^- trimer with interatomic spacings of close to 3.0 Å.[29,30] At higher iodine compositions there was little difference between models with I_3^- or I_5^- species.

III. EXPERIMENTAL RESULTS AND DISCUSSION

A. Diffraction results

Example x-ray intensity contour maps from undoped, 4 mol wt. %, and 45 mol wt. % I_3^--doped P3OT samples are displayed, respectively, in Figs. 2(a), 2(b), and 2(c). Since P3AT's are partially crystalline, only a limited number of Bragg scattering peaks can be distinguished. The most intense of these are located along the equatorial plane ($\ell = 0$) and, in the case of P3OT, include three evenly spaced, low-angle reflections [labeled (200), (400), and (600)] and a broader, higher-angle reflection located near $2\theta = 23.4°$. The low-angle peaks arise from first-, second-, and third-order reflections of the interstack d spacing while the peak labeled (h20) is a superposition of the (020) reflection, which arises from the interlayer chain-to-chain repeat, and other (h20) reflections located on the high-angle side of this peak. The composite sum of these peaks provides for a broad, asymmetric peak. The ability to resolve the individual components has been found to be directly related to the length of the alkyl side chains and to the specifics of the sample quality and its preparation.[19]

The presence of pronounced nonequatorial scattering peaks is indicative of additional structural ordering within individual P3OT stacks. These features are localized along so-called layer lines, parallel to the equatorial plane, at perpendicular distances corresponding to various orders of the nominal P3OT 7.8 Å **c**-axis chain repeat. They may be localized both on and off the meridional (**c**-axis) direction. In this study only scattering within the $\ell = 1$ and $\ell = 2$ was consistently recorded; however, these features are found to extend out to much higher order (up to $\ell = 6$).[20] For pure and very lightly iodine intercalated P3AT films, this scattering intensity always lies off the **c**-axis direction for all odd order ($\ell = 1, 3, 5, ...$) layers. Modeling of this intensity distribution requires a doubling of the 3.8 Å chain-to-chain interlayer repeat (to 7.6 Å) with an average **c**/2 displacement parallel to the chain axis between adjacent alkylthiophene chains. This larger repeat distance a yields nonprimitive orthorhombic unit cell construction. When combined with the tilted orientation of the alkyl side chains, this generates an effective nesting of the alkyl side chains as visualized in Figs. 1(b) and the top of 1(c).

These localized features are always superimposed on a significant background consisting of scattering from the P3OT sample and from the *in situ* assembly. The P3OT noncrystalline background has at least two clearly observable broad scattering halos, one centered at $2\theta \sim 5°$ and the other centered about $2\theta \sim 22°$. The small-angle halo is representative of interchain scattering by polymer chains in "disordered" regions of the film, while the higher-angle halo is identified with the disorder that clearly exists within the alkyl side chain fractions. Because of the complex organization which typifies these hosts, a quantitative of measure of this disorder is not, as yet, possible although a relative qualitative comparison of the overall scattering intensities suggests that a significant proportion of these alkyl side chains is not fully ordered.[31]

The three constant x-ray intensity contour maps in Fig. 2 enable a qualitative comparison of the most ap-

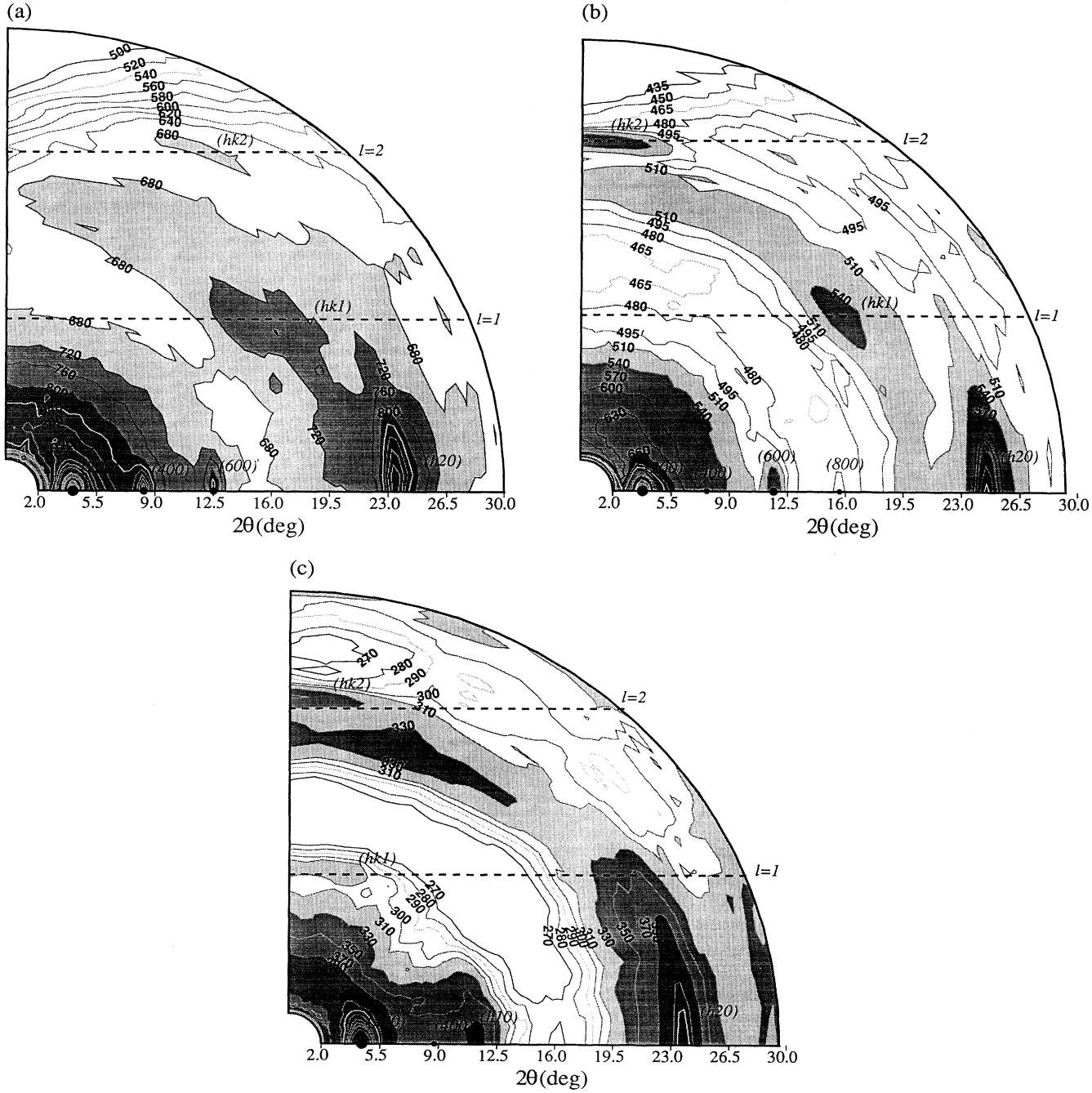

FIG. 2. Contour maps of constant x-ray intensity between the **c** axis and the equatorial ($hk0$) plane for stretch-oriented P3OT at (a) 0, (b) 4, and (c) 45 mol wt. % of I_3^-. In all cases the **c** axis is vertical and the ($hk0$) plane is horizontal. Locations of layer lines have been highlighted for clarity.

parent changes in the scattering profiles which occur during iodine uptake. At very low halogen concentrations, there are pronounced changes in the relative intensities of the equatorial features and a dramatic increase in the scattering intensity along the $\ell = 2$ layer line on and near the meridional direction (i.e., parallel to the **c** axis). The "(002)" scattering intensity reaches a maximum at $2\theta = 22.8°$ and this is indicative of the 3.9 Å spacing of the thiophene rings which comprise the backbone. At moderate to heavy iodine concentrations the off-meridional ($hk1$) scattering diminishes and new features, near the meridian and localized within the $\ell = 1$ layer line, gradually appear. These persistent and continuous variations of the nonequatorial scattering intensities in both the $\ell = l$ and $\ell = 2$ layer lines are suggestive of a continued but evolving interchain structural ordering within individual lamellae. At the highest iodine concentrations, a broad equatorial "($h10$)" feature develops and this is suggestive of a secondary ordering by the iodine intercalant at nearly twice the distance of the chain-to-chain interlayer repeat (typically 7.8 Å).

Selected equatorial ($hk0$) scans, shown in Fig. 3, highlight the positional shifts of the various diffraction peaks. The P3OT host initially displays interlayer and stack interchain spacings of $\mathbf{a}/2 = 20.9$ Å and $\mathbf{b}/2 = 3.82$ Å, respectively. At light to moderate iodine concentrations the ($h00$) reflections move to smaller 2θ while the ($h20$) features are displaced to higher 2θ angles. A clear reversal of this progression can also be seen at the higher iodine levels. The calculated unit cell spacings are shown in Table I. In addition to these equatorial data, a sequence of meridional (or **c**-axis) scans is shown in the inset of Fig. 3. These scans clearly reveal the rapid increase in scattering intensity along the meridional direction for the $\ell = 2$ layer line and the more gradual onset of intensity increases within $\ell = 1$.

Less obvious are the variations in the underlying noncrystalline background. The two slightly anisotropic amorphous halos, centered near 2θ ~5° and 2θ ~22°, shift to higher 2θ angles as iodine uptake ensues. These features also tend to become narrower and even more anisotropic. Moreover, this progression is much more noticeable within the equatorial and meridional profiles than in other, off-axis scans. At the highest iodine concentrations a new, third halo is observed near $2\theta = 30°$. This halo is attributed to the ~ 3 Å intra-iodine scattering signature that would be generated by a distribution of I_n^-, $n = 3, 5, ...$, species that reside in more poorly ordered regions of the polymer film. Similar features have been observed in partially oriented, iodine-doped, polyacetylene films.[29]

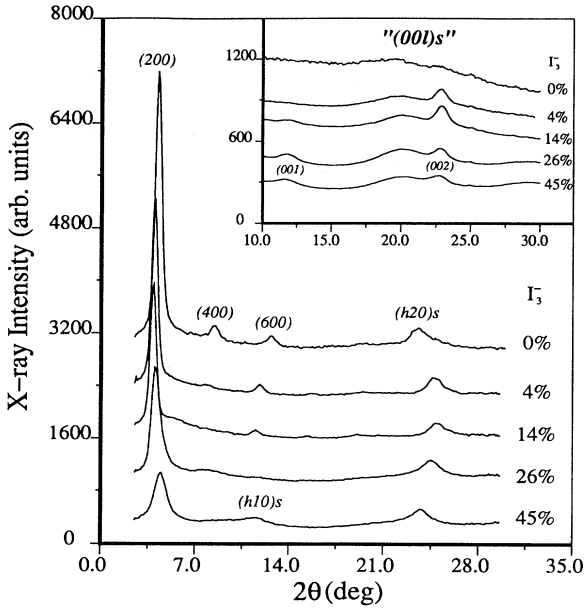

FIG. 3. Experimental equatorial ($hk0$) and **c**-axis (inset) diffraction profiles for P3OT at the various indicated iodine doping levels.

Composite x-ray-scattering spectra, at selected iodine concentrations, are shown in Figs. 4(a)–4(e). These plots display the average integrated x-ray-scattering intensity versus 2θ along each of the scanned layer lines ($\ell = 0$, 1, and 2). These profiles identify additional features not easily distinguished in Figs. 2 or 3. The continued presence of at least two identifiable shoulders on the high-angle side of the ($h20$) peak is indicative of a persistent interlayer ordering, while the localized features along the $\ell = 1$ and $\ell = 2$ layer lines imply intrastack ordering. For $\ell = 2$, there are a number of superimposed peaks in close proximity to the **c**-axis direction. With iodine uptake, the ($hk1$) reflections exhibit a complex behavior and intensify while the ($hk2$) features nearest the **c**-axis direction also become dominant. There is also an appreciable broadening of all radial ($\Delta 2\theta$) peak widths when the I_3^- concentration exceeds 14 mol wt.%. This is the point at which the interlayer spacing now begins to diminish. By 26 mol wt.% of I_3^-, there are no longer any clearly discernable features far off the meridional direction along either $\ell = 1$ or $\ell = 2$ layer lines. This is strongly indicative of pronounced changes in the intrastack chain-

TABLE I. P3OT unit cell parameters.

Lattice parameters				Cell parameters (deg)				Conc. I_3^- (mol wt. %)		I-S dist. (Å)	Chain packing (%)	
a (Å)	**b** (Å)	**c** (Å)	α (deg)	ϕ_R	θ_b	θ_d	$\theta_{b'}$	calc.	expt.	dist.	out-of-phase	in-phase
41.8	7.64	7.81	90.0	9.0	114.0	65.0	0.0	0.0	0.0	NA	100	0
45.1	7.30	7.78	90.0	8.0	108.0	65.0	0.0	4.0	4.0	4.5	100	0
46.3	7.19	7.75	90.0	7.0	103.0	65.0	3.0	16.0	14.0	4.0	64	36
43.0	7.50	7.8	85.0	4.0	110.0	56.0	5.0	21.0	26.0	3.5	11	89
40.5	7.80	7.8	85.0	1.0	113.0	51.0	12.0	45.0	45.0	3.0	0	100

to-chain organization. The unusual shape seen in the "amorphous" halo of the $\ell = 1$ layer line near $2\theta = 25°$ results from a noticeable "leakage" of $\ell = 0$ scattering. Finally, the equatorial ($h10$) feature now appears at this iodine concentration and then becomes gradually more intense with further iodine uptake.

B. Modeling results and discussion

Figures 4(a)–4(e) also display direct comparisons between the calculated scattering profiles from our best-fit models with the experimental data obtained at five representative I_3^- concentrations. In general, very good

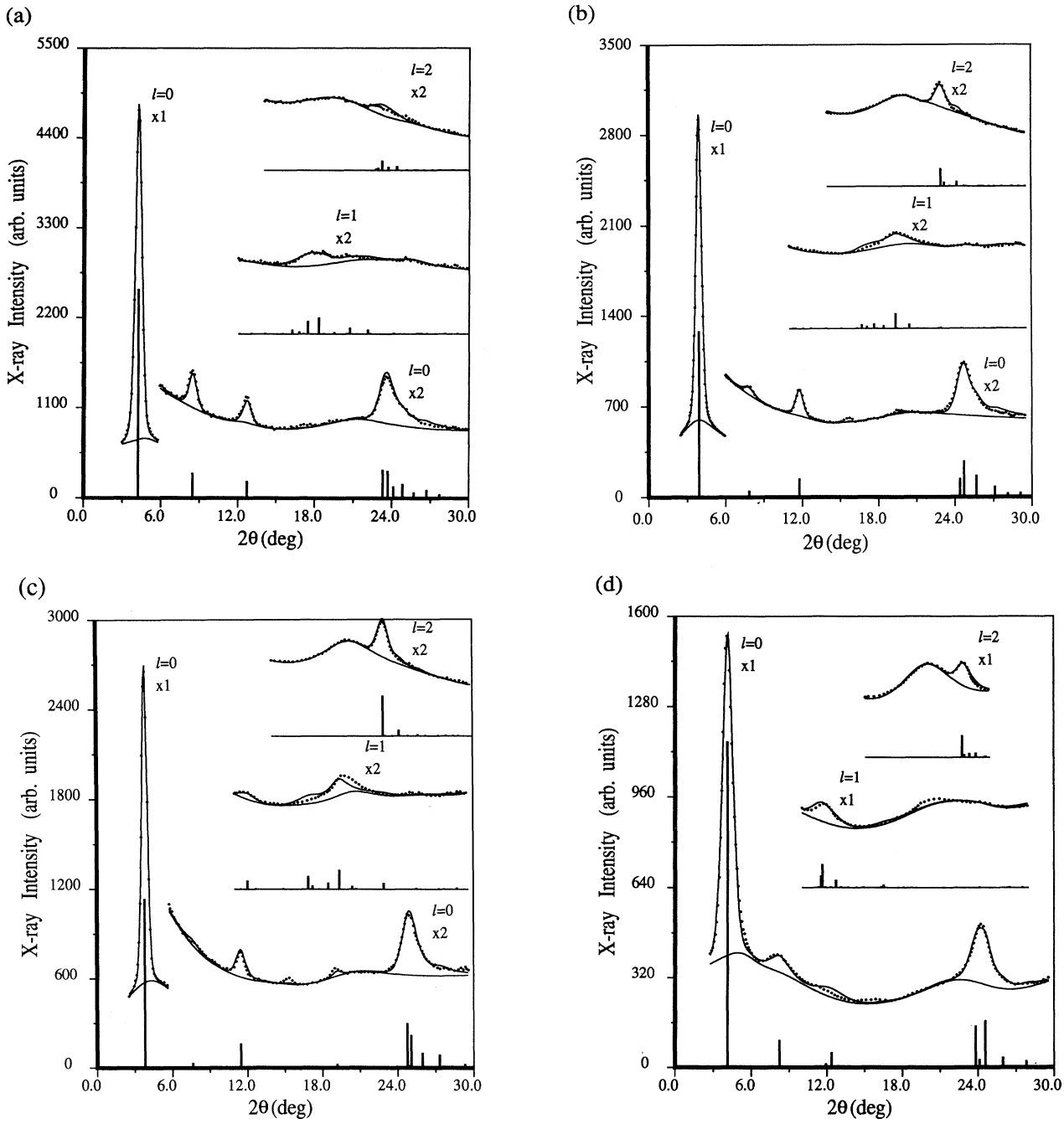

FIG. 4. Comparison of experimental data (dots) and calculated diffraction profiles (lines) at (a) 0 (undoped), (b) 4, (c) 14, (d) 26, and (e) 45 mol wt. % of I_3^- using the parameters listed in Table I. The underlying nonzero Bragg intensities used in the refinement process (vertical bars), as well as the various "amorphous" background profiles are also shown in combination with the zero intensity base lines (horizontal lines). All $\ell \neq 0$ curves have been shifted for clarity.

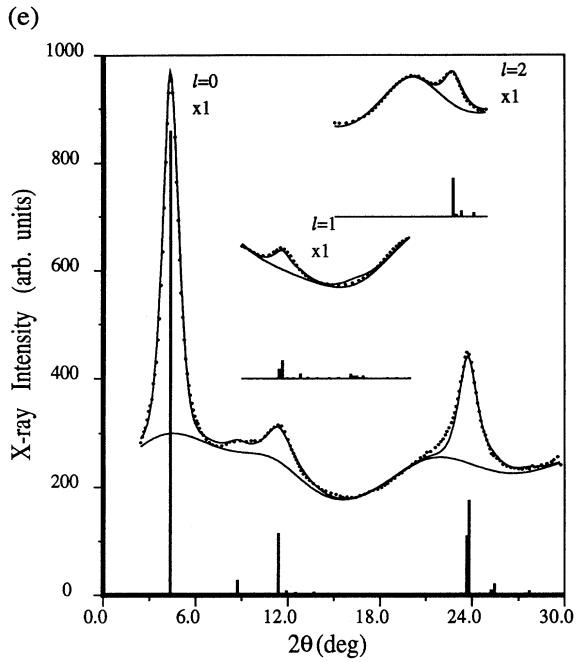

FIG. 4 *(Continued).*

agreement between the experimental and calculated scattering profiles is consistently achieved. To generate these calculated profiles, all individual Bragg reflection intensities have been convoluted with a combined instrumental-sample resolution function and then superimposed on an appropriate (and to some extent arbitrary) background profile. The calculated structure factors typically used only parameters as described in Sec. I. The best-fit base model for pristine P3OT invokes an intrastack layering of individual chains one on top of another such that an alkyl side chain from one polymer chain resides in the gap formed by the mean 7.8 Å spacing of alkyl units along each side of the polymer chain and, thus, enabling an efficient packing arrangement [see the top of Fig. 1(c)]. Similarly, the alkyl chain ends within one layer position themselves to occupy the hollows that are formed at the alkyl chains ends in the adjacent stack. The relative positioning of the chain ends at this interface is subsequently reflected in the weak but reproducible shoulders located on the high-angle side of the high-angle ($2\theta = 23.4°$) equatorial peak.

Within individual P3OT chains the alkyl side chains are found to be strongly oriented out of the plane specified by the alternating all-*trans* planar conformation of the thiophene rings. This average direction is effected in our modeling by first assuming all-*trans* conformation of the alkyl chains and then using the dihedral and bond angles θ_d and θ_b to reorient the side chains. The intent of these two parameters is simply to define the average side chain direction (and not to specify the actual molecular values). As a result, alkyl chains from one stack do not appreciably penetrate (i.e., interdigitate) into those existing in adjacent layers. Models with interdigitation always cause the (400) reflection to become the most intense peak in the calculated structure factor whereas, experimentally, the (200) is always found to be dominant. This pronounced angling of the side chains was also necessary to force the $\ell = 2$ layer line scattering intensity off the **c**-axis direction. At the higher I_3^- concentrations a third side chain parameter $\theta_{b'}$ is found necessary to obtain the best-fit comparisons. This parameter simply rotates the thiophene-octyl side chain C-C bond out of the plane defined by the thiophene ring (perpendicular to the θ_b parameter) and further increases the effective side chain tilt. Other more physical side chain, bond, and dihedral angle variations could be used to achieve the same overall result. The relative positioning of polymer chains within an individual stack is also an important parameter and is essential for matching the position and intensities of peaks along the $\ell = 1$ layer line.

Upon initial exposure to the iodine vapor, the rapid shifts of the (h00) and (h20) peaks to lower and higher 2θ angles, respectively, are strongly correlated with the off-axis to on-**c**-axis intensity variations of the $\ell = 2$ layer line. These observed features are best reproduced in structure factor calculations when the I_3^- anions are allowed to migrate into the gaps between alkyl chains, and orient themselves parallel to the alkyl chain direction, while positioned at distances ranging from 3.5 Å to 4.0 Å from the thiophene-ring sulfur atom. With increasing iodine uptake, both the iodide ions and the side chains are observed to reorient so that they become more nearly perpendicular to the backbone direction. Modeling this behavior yields an intense (002) peak and should, in part, enforce an increase in the intralayer stack repeat. It also appears to increase the amount of open space available to the migrating iodine intercalant ions.

The actual uptake of this iodine into the host matrix has a multitude of specific physical characteristics which are difficult, if not impossible, to accurately model given the complexity of the competing interactions, the intrinsic characteristics of the P3OT host, and the clear limitations of our modeling. Simple hard core packing arguments suggest that the "free" volume within individual intercalant sites is not sufficiently large to allow for a simple intercalant site occupation. Hence as the iodine guest becomes situated within the polymer host, the four closest alkyl chains surrounding any occupied site are likely to be bent or twisted away from the intercalant anion in order to create the necessary space. Alternatively, initial iodine uptake may be facilitated by targeting oversized gaps in the alkyl chain nesting that will necessarily form near chemically disordered (e.g., head-head and tail-tail or equivalently 3-3 and 3′-3′) couplings of the alkyl side chains. It has been established that up to $\sim 25\%$ of the alkyl side chains in these P3OT samples do not have a regiospecific head to tail (3-3′) coupling.[32] Any combination of these effects could account for the mild difficulties encountered in fully reproducing all aspects of the $\ell = 1$ layer line intensity at the lighter iodine concentrations. We note that these aforementioned effects are expected to be most prevalent at the lower iodine concentrations.

As the iodine levels further increase beyond 14 mol wt. % I_3^-, the above structural evolution continues but the changes within the $\ell = 1$ layer line intensity dis-

tribution are most consistent with a model in which there are now net translational motions of the polymer chains in the direction parallel to the main chain axis [see bottom of Fig. 1(c)]. These lateral shifts alter the interlayer stacking and initiate the formation of one-dimensional channels parallel to the **b** axis along either side of the thiophene main chains. Alternating translational motions of ± 1.9 Å per chain are sufficient to bring the entire layer into perfect registry. The percentages of pertinent polymer chains having "in-phase" verses "out-of-phase" stacking are listed in Table I. This **c**-axis translation model has been proposed by Tashiro *et al.*[8] to accommodate the presence of I_5^- in iodine-doped poly(3-hexylthiophene) (P3HT). This motion is consistent with the appearance of the previously forbidden (001) reflection. It is significant to note that the formation of one-dimensional channels is a common structural response to intercalation in linear unsubstituted conducting polymer hosts.[33–37] However, in most guest-host compounds this column formation is parallel to the polymer chain axis whereas in this case there is an analogous response in the *perpendicular* direction. In addition to these translational motions, there are changes in the alkyl orientation with a noticeable increase in θ_b and a net reduction in θ_d. This produces an overall flattening of the polymer stacks. Comparisons between the experimental data and calculations work best when the side chains are stacked so that they obtain a tightly nested arrangement with the neighboring chains (above and below) although the modeling process itself is only sensitive to the average position of side chains and not their exact orientation.

At iodine concentrations near 16 mol wt. % a maximum in the layer spacing occurs. At this point the smooth 2θ positional shifts of the various (h00) and the (h20) peaks reverse direction and there is a rapid onset of broadening in the (h00) reflections. The (200) reflection almost doubles its 2θ width over the I_3^- concentration range from 16 to 20 mol wt. %. With further increases in the iodine content a new equatorial feature, identified as a superposition of (h10) reflections, becomes apparent. All of these equatorial features, as well as the nonequatorial scattering, can be accurately reproduced by our model in this highly intercalated regime. The best agreement between the model and data occurs when the intralayer of stacking of the polymer chains has an "in-phase" alignment of the thiophene rings and alkyl chains to form essentially uninterrupted one-dimensional (1D) columns as described in the last paragraph [see Fig. 1(c)]. The polyiodide anions are now able to interact directly with one another and form stacked arrays in these columns such that the polyiodide anions align themselves perpendicularly to the polythiophene backbone and nearly parallel to the **a** axis of the unit cell. This structural ordering would help to prevent neighboring alkyl side chains from successfully interdigitating. It also enables dopant anions to reside closer to the positively charged backbone and we obtain a minimum iodine-sulfur spacing of ~ 3 Å. As the iodine concentration again increases towards saturation, the I_3^- itself is seen to undergo a secondary ordering so that (h10) repeat becomes a dominant equatorial feature in our P3OT. A similar scattering feature has also been observed in heavily iodine intercalated poly(3-hexylthiophene) samples.[38]

Models with polyiodide anions aligned parallel to the **b** axis[8] (along the 1D channel direction) could not successfully reproduce the observed scattering features. The (h10) feature was especially difficult to reproduce, and modeling doping concentrations were limited to under 33 mol wt. % of I_3^- (or 25 mol wt. % of I_5^-), a value which directly conflicts with the observed concentrations (as high as 79 mol wt. % I_3^- for P3HT). A direct comparison of results from this study and those from an earlier study,[6] where 1D iodine columns were not allowed to form, shows much improved fits to the equatorial scattering data at higher iodine compositions.

At the highest iodine concentrations, there is some indication that neighboring layers, at a distance **a**/2 away, pack such that the alkyl chain ends and the iodine columns both line up creating double-width iodine columns. This relative layer-to-layer positioning of the alkyl side chains between neighboring stacks can be best verified by examining the various (h20) peak intensities. Our data are only weakly suggestive of this structural ordering because of the poor resolution seen in the experimental data on the high-angle side of the (020) peak. The additional contiguous space generated by such an ordering process would efficiently organize the iodine galleries so that intercalant mixtures containing I_5^- and I_7^- species could be more easily accommodated. Alternatively, we note that detailed line shape analysis of the (h00) reflections[39] indicates that the P3AT microcrystallites typically extend only, on average, five layers along the **a**-axis direction (a repeat distance comparable to the more highly ordered P3AT whiskers[12]). Hence a large proportion of the alkyl sides is located at crystal "boundaries" and these larger iodine anions may preferentially congregate within these more open regions.

There is an additional item of significance that may be obtained from these data. The 2θ position of the (002) reflection provides information concerning the **c**-axis thiophene ring repeat distance. This spacing is expected to change during iodine uptake because of the associated charge transfer with the π-conjugated backbone.[40] These changes in the chain repeat distance have been observed in polyacetylene[41,42] and other conducting polymers.[37] In this P3OT study, we observe a slight shift of the (002) peak to slightly higher 2θ angle. Hence there must be a net reduction in the **c**-axis spacing due to this charge-transfer process. However, the precise extent of this movement is difficult to assess because the (002) reflection is extremely weak in the pure P3OT sample and because of the imperfect orientation of these stretch-oriented films. A 0.8% reduction in the **c**-axis spacing is consistent with the observed peak position shifts.

IV. CONCLUSIONS

Understanding the microstructure of conducting polymers is an essential step in achieving the more general goal of fully understanding the physical and electrical properties that these unique materials possess. The abil-

ity to carefully control and monitor the intercalation process of this P3OT/iodine host-guest system has proven to be a key step in advancing the level of information which may be discerned during diffraction studies. These improved data in combination with our enhanced modeling techniques have been able to overcome many of the limitations that are inherent to the study of these highly imperfect host materials. The structural refinement scheme we describe is able to obtain excellent agreement between the *full* three-dimensional scattering intensities generated by the P3OT host polymer and those by various representative structural models for both the pristine state and after intercalation by iodine. We note that the uniqueness of a given structure model is still a potential problem but it is doubtful that, given the known chemical architecture of the host polymer, a significantly different structural modeling scheme can be forwarded which achieves equal success at all levels of iodine intercalation.

The major P3AT structural observation revealed by this study is the singular absence of any significant interdigitation between alkyl side chains in adjacent lamellae at *all* iodine intercalant concentrations. Hence individual layers tend to retain their "individual" identity throughout the intercalation process. Furthermore, the overall structural ordering must be strongly influenced by the nature of the layer interface which forms at regions containing the alkyl chain ends. This modeling has also confirmed a novel translational response by the host polymer chains within individual layers to form essentially one-dimensional intercalant columns. These galleries appear along either side of the polymer backbones and are oriented in a direction perpendicular to the polymer main chain axis. We suggest that this response may be universal in nature with respect to other guest intercalant ion species. This type of local distortion may also appear during the initial uptake of solvents in these and in analogous nonelectroactive hosts materials.[43,44] We also note that this translational motion must effect simultaneous changes in the nature of the p_z overlap by the π orbitals and, thus, will strongly influence any electronic properties that require interchain transport.

The work presented herein represents a small, but significant, step towards developing a fundamental understanding of these complex guest-host structures. Additional studies of intercalation using alternative guest species will further test the "universal" nature of the observed structural response during intercalation. Simultaneous measurement of other physical properties, such as conductivity, taken in parallel with these *in situ* x-ray-diffraction experiments can provide insight into the subtle interrelationships which arise from this complex microstructure. Studies using the highly regiospecific P3AT's are especially appealing for these will eliminate some of the aforementioned problems associated with modeling the alkyl side chemical defects.[45] Regardless, all future proposed P3AT structural models should be rigorously presented in terms of both their peak positions *and* relative intensities if an accurate microscopic model is to be achieved.

ACKNOWLEDGMENTS

Acknowledgment is made to the donors of The Petroleum Research Fund, administered by the ACS, for partial support (T.J.P.) of this research. The financial support by NSF DMR Grant No. DMR-8917530 (M.J.W.) is also gratefully acknowledged.

[1] J. Moulton and P. Smith, Synth. Met. **40**, 13 (1991).
[2] S.-A. Chen and J.-M. Ni, Makromol. Chem. **13**, 31(R) (1992).
[3] S.-A. Chen and J.-M. Ni, Macromolecules **25**, 6081 (1992).
[4] O. Inganas, W. R. Salaneck, H. Osterholm, and J. Laakso, Synth. Met. **22**, 395 (1988).
[5] For the most recent International Conference on Synthetic Metals proceedings, see Synth. Met. **55** (1993).
[6] M. J. Winokur, P. Wamsley, J. Moulton, P. Smith, and A. J. Heeger, Macromolecules **24**, 3812 (1991).
[7] T. J. Prosa, M. J. Winokur, J. Moulton, P. Smith, and A. J. Heeger, Synth. Met. **55**, 370 (1993).
[8] K. Tashiro, Y. Minagawa, M. Kobayashi, S. Morita, T. Kawai, and K. Yoshino, Polym. Prepr. Jpn. **41**, 4595 (1992).
[9] W.-P. Hsu, K. Levon, K.-S. Ho, T. K. Kwei, and A. S. Myerson, Macromolecules **26**, 1318 (1993).
[10] J. Mardalen, E. J. Samuelsen, O. R. Gautun, and P. H. Carsen, Solid State Commun. **77**, 337 (1991).
[11] J. Mardalen, E. J. Samuelsen, O. R. Gautun, and P. H. Carsen, Solid State Commun. **80**, 687 (1991).
[12] K. J. Ihn, J. Moulton, and P. Smith, J. Polym. Sci. Polym. Phys. Ed. **31**, 735 (1993).
[13] T. Kawai, M. Nakazono, and K. Yoshino, J. Mater. Chem. **2**, 903 (1992).
[14] K. Tashiro, K. Ono, Y. Minagawa, M. Kobayashi, T. Kawai, and K. Yoshino, J. Polym. Sci. Polym. Phys. Ed. **29**, 1223 (1991).
[15] A. Bolognesi, M. Catellani, S. Destri, and W. Porzio, Makromol. Chem. **12**, 9(R) (1991).
[16] G. Gustafsson, O. Inganas, H. Osterholm, and J. Laakso, Polymer **32**, 1574 (1991).
[17] T. Kawai, M. Nakazono, R. Sugimoto, and K. Yoshino, J. Phys. Soc. Jpn. **6**, 3400 (1992).
[18] R. McCullough, S. Tristram-Nagle, S. Williams, R. Lowe, and M. Jayaraman, J. Mater. Chem. **2**, 903 (1992).
[19] T. J. Prosa, M. J. Winokur, J. Moulton, P. Smith, and A. J. Heeger, Macromolecules **25**, 4364 (1992).
[20] J. Mardalen, E. J. Samuelsen, O. R. Gautun, and P. H. Carsen, Synth. Met. **48**, 363 (1992).
[21] R. D. McCullough, R. D. Lowe, M. Jayaraman, and D. L. Anderson, J. Org. Chem. **58**, 904 (1993).
[22] R. D. McCullough, R. D. Lowe, M. Jayaraman, P. C. Ewbank, D. L. Anderson, and S. Tristram-Nagle, Synth. Met. **55**, 1198 (1993).
[23] Y. Wei and J. Tian, Macromolecules **26**, 457 (1993).

[24] B. Xu, H. Mao, and S. Holdcroft, Macromolecules **26**, 1163 (1993).
[25] T. Matsuyama *et al.*, Synth. Met. **55**, 690 (1993).
[26] T. Matsuyama, H. Sakai, H. Yamaoka, Y. Maeda, and H. Shirakawa, J. Phys. Soc. Jpn. **52**, 2238 (1983).
[27] P.-A. Albouy, J.-P. Pouget, J. Halim, V. Enkelmann, and G. Weger, Synth. Met. **55**, 690 (1993).
[28] R. Baughman, N. Murthy, G. Miller, and L. Shacklette, J. Chem. Phys. **79**, 1065 (1983).
[29] N. S. Murthy, R. H. Baughman, and G. G. Miller, J. Chem. Phys. **89**, 2523 (1988).
[30] C. D. West, J. Chem. Phys. **15**, 689 (1947).
[31] M. J. Winokur, D. Spiegel, Y. Kim, S. Hotta, and A. J. Heeger, Synth. Met. **28**, C419 (1989).
[32] M. Leclerc, F. M. Diaz, and G. Wegner, Makromol. Chem. **190**, 3105 (1989).
[33] D. Djurado, J. Fischer, P. Heiney, J. Ma, N. Coustel, and P. Bernier, Synth. Met. **34**, 683 (1990).
[34] S. Flandrios, C. Hauw, and B. Francois, Mol. Cryst. Liq. Cryst. **117**, 91 (1985).
[35] R. Baughman, L. Shacklette, N. Murthy, G. Miller, and R. Elsenbaumer, Mol. Cryst. Liq. Cryst. **118**, 253 (1985).
[36] L. Shacklette and J. Toth, Phys. Rev. B **32**, 5892 (1985).
[37] D. Chen, M. Winokur, M. Masse, and F. Karasz, Phys. Rev. B **41**, 6759 (1990).
[38] M. J. Winokur, T. J. Prosa, J. Moulton, P. Smith, and A. J. Heeger, Polymer **33**, 296 (1992).
[39] T. J. Prosa, M. J. Winokur, J. Moulton, P. Smith, A. J. Heeger, and R. D. McCullough (unpublished).
[40] S. Hong and M. Kertesz, Phys. Rev. Lett. **64**, 3031 (1990).
[41] M. Winokur, Y. Moon, A. Heeger, J. Barker, and D. Bott, Solid State Commun. **68**, 1055 (1988).
[42] D. Begin, M. Lelaurain, and D. Billaud, Mater. Sci. Forum **91**, 357 (1992).
[43] M. Ballauff and K. Berger, Mol. Cryst. Liq. Cryst. **1557**, 109 (1988).
[44] M. Ballauff, R. Rosenau-Eichin, and E. Fischer, Mol. Cryst. Liq. Cryst. **155**, 211 (1988).
[45] R. D. McCullough, S. Tristram-Nagle, S. P. Williams, R. D. Lowe, and M. Jayaraman, J. Am. Chem. Soc. **115**, 4910 (1993).

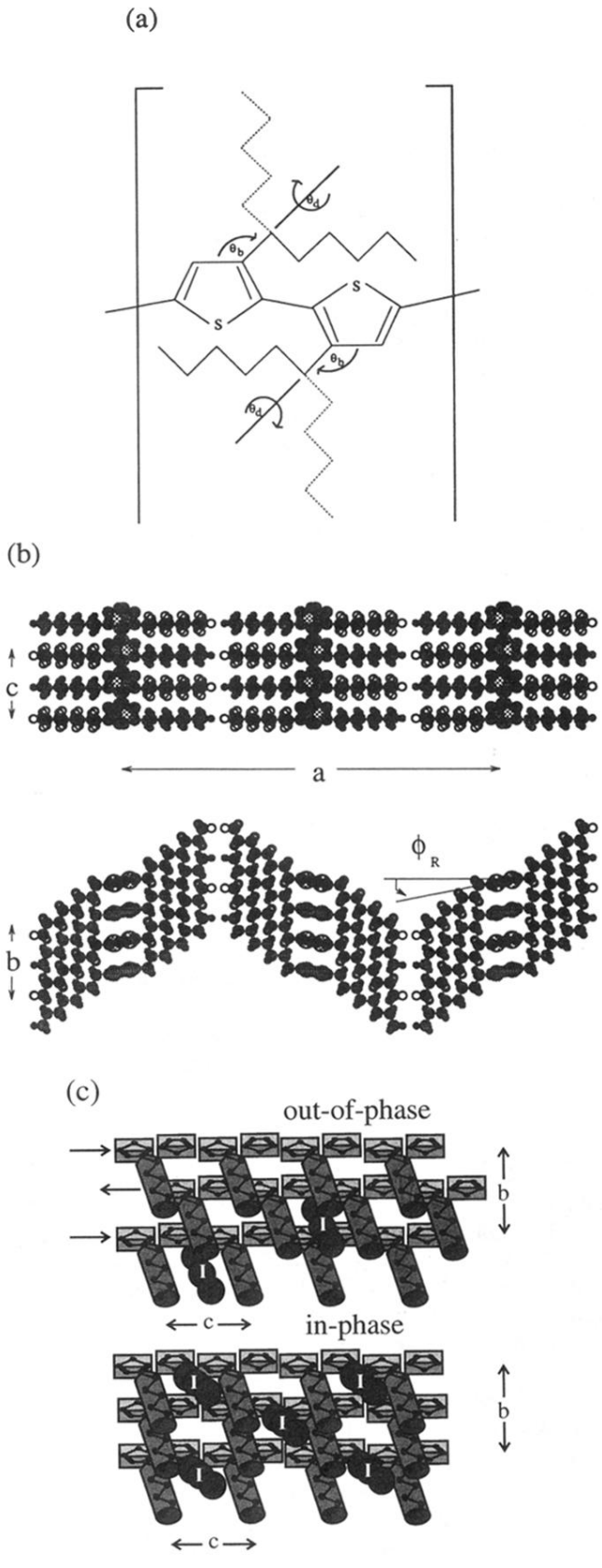

FIG. 1. Various views of P3OT structure and the modeling degrees of freedom: (a) The chemical structure of P3OT; (b) two different projections of the P3OT lamellar packing; (c) packing of side chains for undoped lightly doped (top) and heavily doped P3OT (bottom).

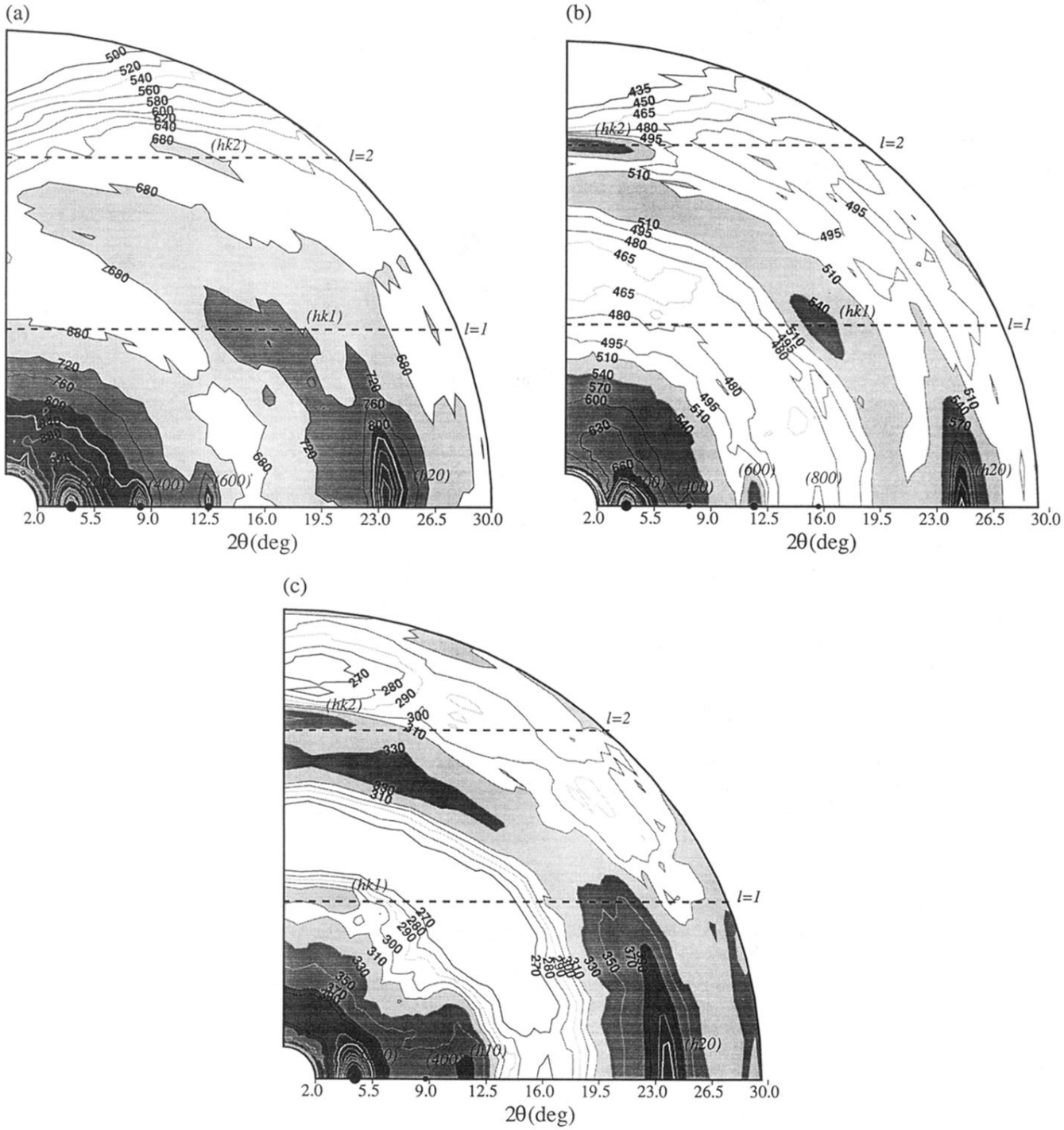

FIG. 2. Contour maps of constant x-ray intensity between the **c** axis and the equatorial ($hk0$) plane for stretch-oriented P3OT at (a) 0, (b) 4, and (c) 45 mol wt. % of I_3^-. In all cases the **c** axis is vertical and the ($hk0$) plane is horizontal. Locations of layer lines have been highlighted for clarity.